



**INORGANIC
CHEMISTRY**
FRONTIERS

**A Proof-of-Concept Application of Water-Soluble
Ytterbium(III) Molecular Probes for *In Vivo* NIR-II Whole
Body Bioimaging**

Journal:	<i>Inorganic Chemistry Frontiers</i>
Manuscript ID	QI-RES-02-2019-000157.R1
Article Type:	Research Article
Date Submitted by the Author:	05-May-2019
Complete List of Authors:	Ning, Yingying; Peking University, College of Chemistry and Molecular Engineering Chen, Si; Stanford University, Department of Radiology Chen, Hao; Stanford University, Department of Radiology Wang, Jing-Xiang; Peking University, College of Chemistry and Molecular Engineering He, Shuqing; Stanford University, Department of Radiology Liu, Yi-Wei; Peking University, College of Chemistry and Molecular Engineering Cheng, Zhen; Stanford University, Department of Radiology Zhang, Jun-Long; Peking University, College of Chemistry and Molecular Engineering

SCHOLARONE™
Manuscripts



Journal Name

ARTICLE

A Proof-of-Concept Application of Water-Soluble Ytterbium(III) Molecular Probes for *In Vivo* NIR-II Whole Body Bioimaging

Yingying Ning,^{‡,a} Si Chen,^{‡,b,c} Hao Chen,^b Jing-Xiang Wang,^a Shuqing He,^b Yi-Wei Liu,^a Zhen Cheng^{*,b} and Jun-Long Zhang^{*,a}

Received 00th January 20xx,
Accepted 00th January 20xx

DOI: 10.1039/x0xx00000x

www.rsc.org/

Near-infrared (NIR) emissive lanthanide (Ln) complexes are promising candidates for fluorescence imaging in NIR-II region (1000-1700 nm) to combine the advantages of small organic molecules and inorganic metal ions. However, their metabolism *in vivo* and applications for *in vivo* imaging are still unknown. In this work, we used water-soluble Yb³⁺ molecular probes with the quantum yields of ca. 10% in water, which showed deep penetration depth (>3 mm) upon excitation at Q band. One of the Yb³⁺ complexes, **Yb-2**, was successfully applied in high resolution non-invasive whole body, vasculature and lymph node imaging of small animals. The complex cleared from the body through hepatobiliary and renal systems, similar to most organic fluorophores. Importantly, we demonstrated the application of **Yb-2** in fluorescence-guided sentinel lymph node surgery, showing the perspective application of lanthanide complexes as molecular probes in NIR-II whole body bioimaging and surgical operation.

Introduction

Fluorescence imaging allows non-invasive, sensitive and high resolution monitoring of many early events in carcinogenesis and wide-range biological processes *in vivo*. Compared to traditional fluorescence imaging in the visible and NIR-I region (400-900 nm), imaging at the second near-infrared window (NIR-II, 1000-1700 nm) dramatically reduced tissue absorption and autofluorescence and photon scattering.^{1,2} Consequently, fluorescent imaging in the NIR-II window can achieve deeper tissue penetration depth and higher spatial and temporal resolution than those in NIR-I window.^{3,4} In recent years, organic molecules,⁵⁻⁸ carbon nanotubes,⁹ quantum dots^{10,11} and upconversion nanoparticles¹²⁻¹⁴ have been used for NIR-II *in vivo* imaging, particularly in the real-time vasculature visualization and removal of sentinel lymph nodes and tumors. However, organic dyes generally suffer from the problems such as easy photobleaching and small Stokes shift; on the other side, inorganic nanomaterials are limited by their unknown toxicity concerns and slow excretion pharmacokinetics arising from the sizes.^{15,16}

To circumvent the photostability of organic molecules and large size in inorganic nanoparticles, NIR-II emissive lanthanide (Ln) complexes are promising candidates for their small sizes and metal-centered emission.^{17,18} These features endow them f-f characteristic emission, large Stokes shift and high photo- and/or chemostability.^{19,20} However, Ln NIR luminescence is easily quenched by high energy X-H bond (X = C, N and O) vibration arising from ligands and solvents.²¹⁻²³ Only very limited number of NIR Ln molecular probes have previously been applied in cell imaging due to the low quantum yields (below 3% in water),²⁴⁻²⁸ although many visible Ln molecular probes have been investigated for bioimaging before.²⁹⁻³³ Even up to date, *in vivo* imaging using NIR Ln molecular probes with antenna ligand has not been achieved for the inefficient antenna effect, although the design of NIR probes for bioanalysis have been started two decades ago.³⁴⁻³⁶ To overcome this challenge, we recently reported perfluorinated Yb³⁺ porphyrinates emitted with unprecedented high quantum yields (ca. 25%) in NIR region (900-1100 nm).^{37,38} Moreover, after subsequent modifications to improve the biocompatibility, the quantum yields of Yb³⁺ complexes reached 5-13% in water, so that they can be applied in living cell imaging.³⁹ Their long decay lifetimes also make them successfully applied in time-resolved fluorescence lifetime imaging recently.⁴⁰ However, the behaviour of the Yb³⁺ complexes *in vivo* was still unknown. Therefore, the next endeavour is to answer the crucial questions such as whether Yb³⁺ porphyrinates can be employed in NIR-II *in vivo* whole body bioimaging, which is critical to demonstrate their potential applications as theragnostic agents eventually for clinical translation.

^a Beijing National Laboratory for Molecular Sciences, State Key Laboratory of Rare Earth Materials Chemistry and Applications, College of Chemistry and Molecular Engineering, Peking University, Beijing 100871, P. R. China

^b Molecular Imaging Program at Stanford (MIPS), Bio-X Program, and Department of Radiology, Canary Center at Stanford for Cancer Early Detection, Stanford University, California 94305-5344, USA

^c Department of Neurology, Xiangya Hospital, Central South University, Xiangya Road 88, Changsha, Hunan 410008, P.R. China

[‡] These authors contributed equally.

Electronic Supplementary Information (ESI) available: [details of any supplementary information available should be included here]. See DOI: 10.1039/x0xx00000x

Herein we reported a proof-of-concept work using water-soluble Yb³⁺ molecular probes for *in vivo* whole body bioimaging. According to previous report, we synthesized cationic phosphoniums³⁹ and anionic carboxylate Yb³⁺ porphyrinates⁴⁰ with quantum yields of ca. 10% in water. Combing with the large extinction coefficient of porphyrin ligand, **Yb-2**, with carboxylate modification, presents high *in vivo* luminescence and achieves high resolution vasculature imaging in small animals. By using a 1000 nm longpass, the Yb³⁺ porphyrinate has been demonstrated to help the image-guided operation in NIR-II region using mice models. Therefore, this work provides a foundation and insight to the design of NIR *in vivo* imaging molecular probes using emissive Ln coordination compounds and enriches the repertoire of Ln-compounds chemical biology.

Results and Discussion

According to previous report, we prepared **Yb-2** and **Yb-3** as water-soluble Yb³⁺ porphyrinates with carboxylate and cationic phosphoniums, respectively (Fig. 1a).^{39, 40} **Yb-1** was used as control and kept the ester group, not water-soluble. The absorption spectra of Yb³⁺ complexes in DMSO and H₂O are similar and display with the intense Soret band centered at ca. 410 nm and Q bands between 520-650 nm (Fig. 1b and S1). It is noteworthy that the extinction coefficient (ϵ) of Q band in

the range of ca. 525-620 nm is larger than $10^4 \text{ M}^{-1}\text{cm}^{-1}$ for **Yb-2**. Upon excitation at Soret or Q band, **Yb-1-3** exhibited intense characteristic ${}^2\text{F}_{5/2} \rightarrow {}^2\text{F}_{7/2}$ transition bands of Yb³⁺ at 900–1100 nm. The fluorescence quantum yields of **Yb-1-3** in DMSO were ca. 20-22%, with the long decay lifetimes of ca. 205-220 μs (Fig. S2). Importantly, compared to **Yb-3** ($\Phi_{\text{Yb}} = 5.1\%$, $\tau_{\text{obs}} = 56 \mu\text{s}$ in H₂O), **Yb-2** presented higher quantum yield (10%, Fig. 1c) and lifetime (140 μs) in H₂O (Fig. S3), with the brightness ($\epsilon \cdot \Phi$) of ca. $10^3 \text{ M}^{-1}\text{cm}^{-1}$. Although complex **Yb-2** is pH-sensitive, the complex still maintains high luminescence and lifetime (100 μs) in serum. For **Yb-3**, the NIR emission is not pH-sensitive (Fig. S4). More importantly, from the NIR-II images in water (Fig. 1d), we can observe strong NIR-II luminescence from **Yb-2** and **Yb-3** even under the excitation at 520 nm (Q band).

The **Yb-2** and **Yb-3** showed high stability in water, phosphate buffer saline (PBS), and fetal bovine serum (FBS) under basic and acidic conditions (Fig. S5-6). Importantly, we found that the complexes showed significant higher photostability than commercial NIR fluorophore (Cy5.5), when taking **Yb-2** as an example (Fig. S7). Although the complexes showed lower NIR brightness than that of Cy 5.5 (ca. $10^4 \text{ M}^{-1}\text{cm}^{-1}$), they are still promising for *in vivo* imaging due to the strong resistance to photobleaching. Standard CCK-8 assay also indicated the low dark cytotoxicity and photocytotoxicity of **Yb-2** and **Yb-3** towards HeLa cells (Fig. S8).

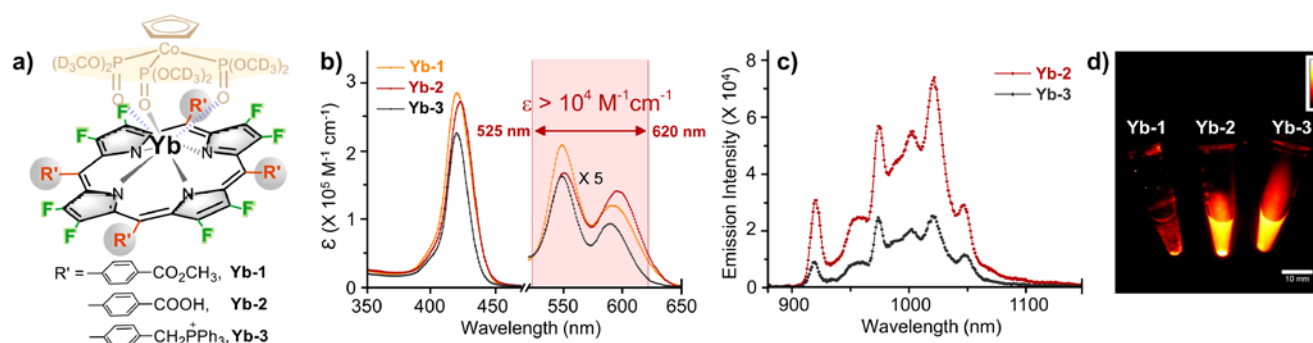


Fig. 1 a) Structures of the Yb³⁺ complexes studied in this work. b) Normalized absorption spectra of **Yb-1-3** in DMSO; c) Emission spectra of **Yb-2** and **Yb-3** in water ($\lambda_{\text{exc}} = 410 \text{ nm}$, $A_{410 \text{ nm}} = 0.1$); d) NIR-II fluorescence image of an aqueous solution of **Yb-1** to **Yb-3** under the excitation of 520 nm (1000 nm longpass).

As **Yb-2** shows higher NIR quantum yield than **Yb-3**, before application for *in vivo* bioimaging, we investigated the NIR-II penetration depth by covering pork of different thickness (0, 4, 8 mm) on the water solution of **Yb-2** as an example. As shown in Fig. 2, upon excitation at Q band (532 nm), the NIR-II luminescence signals decreased with the increasing of pork thickness and decreasing of excitation laser power. However, the signals were still collected even with the block of 8 mm pork and using 50 mW/cm² excitation laser power, which should benefit from the high luminescence of **Yb-2**. These results strongly demonstrate the deep penetration ability of the **Yb-2** luminescence in NIR-II region.

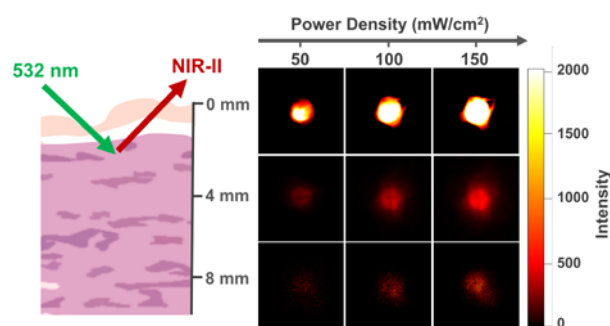


Fig. 2 Luminescence intensity of **Yb-2** (2 mg/mL) in the NIR-II region (100 ms exposure, 1000 nm longpass) under corresponding penetration depth (0, 4, 8 mm) and excitation laser power (532 nm, 50, 100 and 150 mW/cm²).

Based on *in vitro* results, we then performed whole-body NIR-II imaging of C57BL/6 mice with the injection of **Yb-2** using 1000 nm longpass under excitation of 520 nm laser. Immediately after tail vein injection, superior vasculature and whole body imaging was visualized from the surrounding background tissue, due to the reduced scattering, tissue absorption and autofluorescence in the NIR-II window, as shown in Fig. 3. After 12 h post-injection, *ex vivo* biodistribution study was performed to evaluate the biodistribution of the complex in major organs. The results showed that **Yb-2** mainly accumulated in kidneys and intestine. A small fraction of probe signal was also detected in liver and no signals were observed in muscle, matching with the *in vivo* fluorescence results. These indicate that the clearance routes of the Yb^{3+} complex is through both hepatobiliary and renal systems, similar to most organic fluorophores.^{1, 41} NIR-II fluorescence images were also captured on the 143B osteosarcoma tumor-bearing mouse after **Yb-2** injection intravenously and no osteosarcoma fluorescence images were observed (Fig. S9). This indicated that the complexes are still needed to be further modified to be tumor targeting. However, after 36 h tail vein injection, imaging of femoral artery and major artery could still be observed (Fig. S10), suggesting the long blood-circulation half-life of **Yb-2**. The high stability and long excretion time provides the possibility of utilizing the Yb^{3+} complexes for real-time visualization in long-time surgical operation, clinical diagnoses and biopsy.

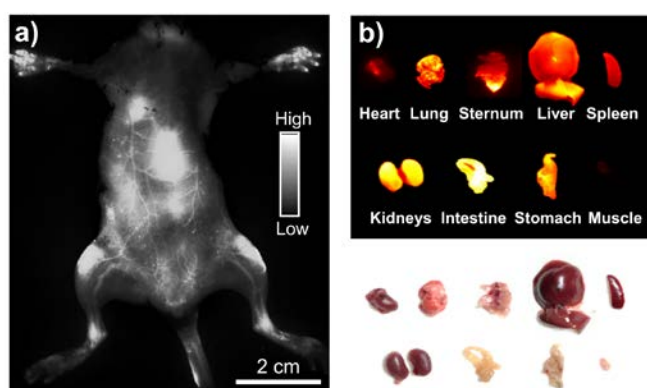


Fig. 3 a) Whole body NIR-II fluorescence images of **Yb-2** (150 μL , 3 mg/ml) after 5 min intravenous injection into C57BL/6 mice (λ_{ex} , 520 nm; λ_{em} , 1000 nm longpass; 3000 ms exposure; colour bar ranges from 5000 to 40,000, $n = 3$ per group); b) *Ex vivo* biodistribution studies at 12 h after injection of **Yb-2**.

Then we compared the NIR-II *in vivo* imaging resolution between **Yb-2** and **Yb-3** under the same conditions. Immediately after tail vein injection (150 μL , 3 mg/ml), NIR-II fluorescence images of the mice were captured. As shown in Fig. 4, NIR-II image using **Yb-2** (Fig. 4a) displayed more small vessels compared to that obtained by **Yb-3** (Fig. 4b). The Gaussian-fit of the vessel FWHM (full width at half maxima) width is ca. 250.03 μm , with the signal-to-background ratio (SBR) of 2.49 ± 0.3 (Fig. 4c). However, compared to **Yb-2**, NIR-II image of blood vessel using **Yb-3** showed significant lower resolution (FWHM = 504.24 μm) and signal to background

ratio (1.37 ± 0.1 , Fig. 4d), likely due to the lower NIR quantum yield. This indicates the importance of NIR quantum yields on the *in vivo* imaging resolution in NIR-II region. Although the value of signal to background ratio is still slightly lower than that obtained using NIR-II luminescent organic molecules,^{7, 42} which should be due to the visible excitation wavelength, this can be improved by precise modulation of the porphyrin structures in the future.^{24, 43}

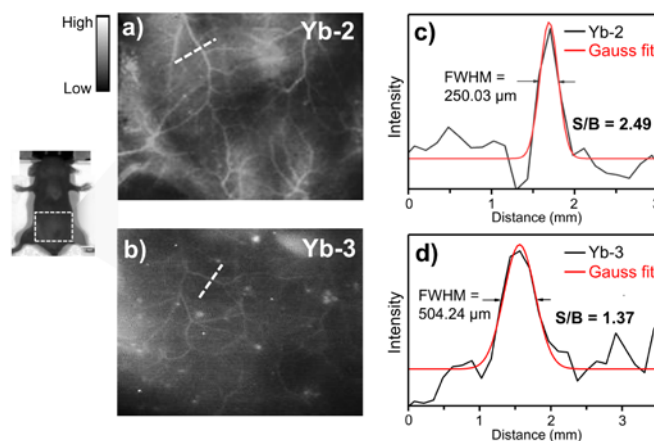


Fig. 4 Vasculature images of a) **Yb-2** and b) **Yb-3** (150 μL , 3 mg/ml) after 5 min intravenous injection into C57BL/6 mice (λ_{ex} , 520 nm; λ_{em} , 1000 nm longpass; 3000 ms exposure; colour bar ranges from 5000 to 40,000, $n = 3$ per group). Vessel FWHM width (white lines in a) and b) and SBR analysis of c) **Yb-2** and d) **Yb-3**, based on the cross-sectional intensity profiles.

Considering the higher resolution and SBR of **Yb-2** than **Yb-3**, we chose **Yb-2** for further *in vivo* experiments. **Yb-2** was then injected in footpads of nude mice in a prone position to explore the application in lymphoscintigraphy. One hour after the injection, high-bright contrast of lymphatic vasculature and nodes were visualized clearly (Fig. 5). The popliteal lymph node-to-background ratios were observed as 7.95 ± 0.3 and remained as high as 6.8 ± 0.2 even after 12 h injection. Moreover, the NIR-II measured lymph vessel had a Gaussian-fit diameter of ca. 591.7 μm and SBR of ca. 2.59 ± 0.1 at 1 h, reflecting the transportation of the complex through lymphatic system. This revealed the potential application of the Yb^{3+} complex in lymph related diagnoses and surgical operation.

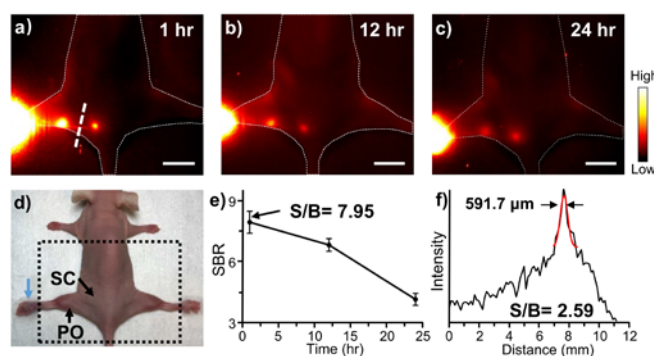


Fig. 5 a), b), c) NIR-II fluorescent image ~1, 12, 24 hours post-injection of 3mg/ml **Yb-2** injected in left foot and PBS in right foot (λ_{ex} , 520 nm; λ_{em} , 1000 nm longpass; 3000 ms exposure; colour bar ranges from 100 to 25,000). d)

Photograph depicting nude mouse in prone position for imaging popliteal and sacral lymph nodes in a), b), c). Fluorophore injection sites indicated by blue arrows next to footpad. e) The popliteal lymph node-to-background ratios was determined with different time after **Yb-2** injection. f) The FWHM width and SBR (white lines in a)) analysis of the lymph vessel, basing on the fluorescent cross-sectional intensity profiles. Scale bar: 1 cm.

NIR-II fluorophores have showed the advantages in the real-time removal of sentinel lymph nodes and tumors for the higher spatial and temporal resolution, which is potential to "imaging-guided-operation".^{1, 2} Due to the high popliteal lymph node-to-tissue ratios of **Yb-2**, we then carried out the surgical resection of popliteal and sacral lymph nodes under the guidance of NIR-II imaging. As shown in Fig. 6, distinguished by the higher fluorescence intensity, the popliteal and sacral lymph nodes can be easily and clearly identified and dissected at their prone position under the NIR-II imaging, successfully mimicking the standard SLNB procedure of clinical cancer surgery. Importantly, after the lymph nodes were resected, the operative field was clearly identified with NIR-II imaging, proving no lymph nodes were remained.

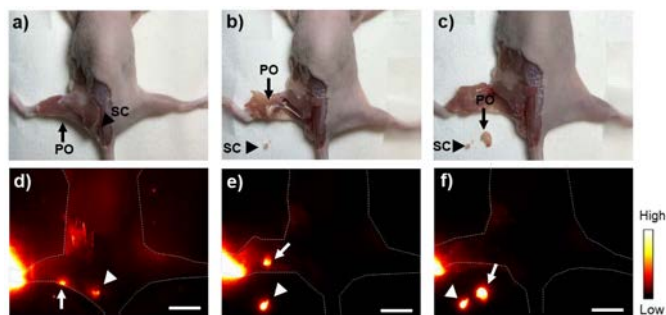


Fig. 6 *In vivo* NIR-II image-guided popliteal and sacral lymph nodes mapping and biopsy. NIR-II fluorescent image at ~24 hours post-injection of 3 mg/ml **Yb-2** injected in left foot of nude mice ($n = 3$ per group; λ_{ex} , 520 nm; λ_{em} , 1000 nm longpass; 1000 ms exposure; colour bar ranges from 1200 to 50,000). a), b), c) Photograph depicting a nude mouse in prone position for imaging popliteal (black arrow) and sacral (black arrowhead) lymph nodes in dissecting the skin in a), then dissecting the muscle and exposed the lymph nodes in b) and c). d), e), f) The popliteal (white arrow) and sacral (white arrowhead) lymph nodes were clearly identified and dissected at their precise position in a short time. Scale bar: 1 cm.

Conclusions

Taken together, we utilized highly luminescent water-soluble β -fluorinated Yb^{3+} complex for *in vivo* NIR-II whole body bioimaging. Because of the deep penetration depth of the Yb^{3+} luminescence, complex **Yb-2** was successfully applied in noninvasive imaging of mice blood and lymphatic vasculatures, and image-guided sentinel lymph node surgery in NIR-II region, achieving high signal-to-noise ratio. The metabolism mechanism of the Yb^{3+} complex *in vivo* is similar to small organic molecules, excluding the slow excretion disadvantage of nanoparticles. As the luminescence of lanthanide complex is metal-centered, it possesses higher photostability and environment irrelevant emission bands than traditional

organic dye. These results indicate that lanthanide complexes are highly promising and clinically translatable NIR-II fluorescence probes, paving a way to the design of metal coordination complexes for NIR-II fluorescence imaging and the study of NIR Ln^{3+} *in vivo* biology. Red-shifting the excitation wavelength to NIR region and achieving tumor targeting are highly desirable in the next step, which are also currently under exploration in our lab.

Experimental Section

General materials and methods

Unless otherwise stated, all reactions were performed under an inert atmosphere of nitrogen. UV-vis spectra were recorded on an Agilent 8453 UV-vis spectrometer equipped with an Agilent 89090A thermostat (± 0.1 °C) at 25 °C. HeLa cells were obtained from Peking University Health Science Center and incubated in complete medium (Dulbecco's modified Eagle's Medium, supplemented with 10% fetal bovine serum (FBS) and 1% penicillin-streptomycin) at 37 °C in atmosphere containing 5% CO_2 . Eight-week-old male C57BL/6 mice and nude mice were obtained from Charles River for animal studies and all animal procedures were performed under the approval of Stanford University's Administrative Panel on Laboratory Animal Care. For the optical measurements in liquid solution, spectroscopic-grade dimethyl sulfoxide was used as purchased from Alfa-Aesar. H_2O were obtained from Milli-Q integral. **Yb-1**, **Yb-2** and **Yb-3** were synthesized according to literature methods.^{39, 40}

Photophysical properties measurements

Emission, excitation spectra and lifetime were measured on an Edinburgh Analytical Instruments FLS980 lifetime and steady state spectrometer equipped with a 450 W Xe lamp, a 60 W microsecond flash lamp, PMT R928 for visible emission spectrum, HAMAMATSU R5509-73 PMT with C9940-02 cooler for NIR emission spectrum and luminescence lifetime. Excitation and emission spectra were corrected for instrumental functions (including the correction for detector, gratings etc). Quantum yields were determined using comparative method,⁴⁴ similar to previous studies.³⁹ The estimated error for the quantum yield measurements is 15%.

Cytotoxicity assay

HeLa cells were seeded in flat-bottomed 96-well plates, 10^4 cells per well, with 200 μL complete culture media in the dark for 24 h. Cells were incubated with 1-16 μM complexes for another 24 h in the dark while wells containing no cells are set as the controls. (for the measurement of photocytotoxicity: after washed three times with PBS, the cells were irradiated for 30 min in 100 μL PBS under the light irradiation (400–700 nm) with the same dose of light (6.5 mW/cm^2) for 30 min. Then PBS was replaced by 200 μL fresh culture media.) After cultured for 24 h, the cells were washed three times with PBS. Then 10 μL Cell Counting Kit-8 (CCK-8) solution and 90 μL PBS

were added per well. After 30 min, the absorbance at 450 nm was read by 96-well plate reader. The viability of HeLa cells was calculated by the following equation:

$$CV = (A_s - A_b) / (A_c - A_b) \times 100\% \quad (1)$$

CV stands for the viability of cells, A_s , A_c and A_b stand for the absorbance of cells containing the studied complexes, cell control (no treated cells) and blank control (wells containing neither cells nor the studied complexes).

In vivo NIR-II fluorescence imaging

Mice were placed on a stage with a venous catheter for injection of contrast and imaging agents, anesthetized using a 2 L/min oxygen flow with 2% Isoflurane. The excitation laser was a 520 nm laser diode at a power density of 0.3 W/cm² and emission was collected using two-dimensional InGaAs array (Princeton Instruments) with a 1000 nm longpass filter. A lens set was used to obtain tunable magnifications ranging from 1× (whole body) to 2.5× (high magnification) magnification by changing the relative position of two NIR achromats (200 mm and 75 mm, Thorlabs). The exposure time for all images was 1000-3000 ms and images were processed with Image J.

Ex vivo biodistribution analysis

12 h after injection of **Yb-2**, nude mice were sacrificed and the major organs and tissues were collected. Then the NIR-II fluorescence images were obtained using a home-built NIR-II fluorescence imaging system with an InGaAs camera under illumination of a 520 nm laser diode at a power density of roughly 50 mW/cm² and an exposure time of 500 ms.

Conflicts of interest

There are no conflicts to declare.

Acknowledgements

We acknowledge financial support from the National Key Basic Research Support Foundation of China (2015CB856301), National Scientific Foundation of China (Grants NO. 21778002, 21571007, 21861162008 and 81301160), the Office of Science (BER), U.S. Department of Energy (DE-SC0008397), and NCI of Cancer Nanotechnology Excellence Grant CCNE-TR U54 CA119367, CA151459.

Notes and references

- G. Hong, A. L. Antaris and H. Dai, *Nat. Biomed. Eng.*, 2017, **1**, 0010.
- Q. Miao and K. Pu, *Adv. Mater.*, 2018, **30**, 1801778.
- S. He, J. Song, J. Qu and Z. Cheng, *Chem. Soc. Rev.*, 2018, **47**, 4258-4278.
- Y. Jiang and K. Pu, *Adv. Biosys.*, 2018, **2**, 1700262.
- A. L. Antaris, H. Chen, K. Cheng, Y. Sun, G. Hong, C. Qu, S. Diao, Z. Deng, X. Hu, B. Zhang, X. Zhang, O. K. Yaghi, Z. R. Alamparambil, X. Hong, Z. Cheng and H. Dai, *Nat. Mater.*, 2016, **15**, 235-242.
- E. D. Cosco, J. R. Caram, O. T. Bruns, D. Franke, R. A. Day, E. P. Farr, M. G. Bawendi and E. M. Sletten, *Angew. Chem. Int. Ed.*, 2017, **56**, 13126-13129.
- Q. Yang, Z. Hu, S. Zhu, R. Ma, H. Ma, Z. Ma, H. Wan, T. Zhu, Z. Jiang, W. Liu, L. Jiao, H. Sun, Y. Liang and H. Dai, *J. Am. Chem. Soc.*, 2018, **140**, 1715-1724.
- Y. Jiang, P. K. Upputuri, C. Xie, Y. Lyu, L. Zhang, Q. Xiong, M. Pramanik and K. Pu, *Nano Lett.*, 2017, **17**, 4964-4969.
- H. Gong, R. Peng and Z. Liu, *Adv. Drug. Deliv. Rev.*, 2013, **65**, 1951-1963.
- C. Chen, P. Zhang, G. Gao, D. Gao, Y. Yang, H. Liu, Y. Wang, P. Gong and L. Cai, *Adv. Mater.*, 2014, **26**, 6313-6317.
- M. Sakiyama, H. Sugimoto and M. Fujii, *Nanoscale*, 2018, **10**, 13902-13907.
- Y. Lu, J. Lu, J. Zhao, J. Cusido, F. M. Raymo, J. Yuan, S. Yang, R. C. Leif, Y. Huo, J. A. Piper, J. Paul Robinson, E. M. Goldys and D. Jin, *Nat. Commun.*, 2014, **5**, 3741.
- W. Zheng, D. Tu, P. Huang, S. Zhou, Z. Chen and X. Chen, *Chem. Commun.*, 2015, **51**, 4129-4143.
- Y. Fan, P. Wang, Y. Lu, R. Wang, L. Zhou, X. Zheng, X. Li, J. A. Piper and F. Zhang, *Nat. Nanotechnol.*, 2018, **13**, 941-946.
- I. Martinić, S. V. Eliseeva and S. Petoud, *J. Lumin.*, 2017, **189**, 19-43.
- E. Thimsen, B. Sadtler and M. Y. Berezin, *Nanophotonics*, 2017, **6**, 1043-1054.
- J.-C. G. Bünzli, *J. Lumin.*, 2016, **170**, 866-878.
- C. G. Ma, M. G. Brik, D. X. Liu, B. Feng, Y. Tian and A. Suchocki, *J. Lumin.*, 2016, **170**, 369-374.
- D. Parker, in *Handbook on the Physics and Chemistry of Rare Earths*, Elsevier, 2016, vol. 50, pp. 269-299.
- M. Sy, A. Nonat, N. Hildebrandt and L. J. Charbonniere, *Chem. Commun.*, 2016, **52**, 5080-5095.
- G. Mancino, A. J. Ferguson, A. Beeby, N. J. Long and T. S. Jones, *J. Am. Chem. Soc.*, 2005, **127**, 524-525.
- C. Doffek, N. Alzakhem, C. Bischof, J. Wahsner, T. Guden-Silber, J. Lügger, C. Platas-Iglesias and M. Seitz, *J. Am. Chem. Soc.*, 2012, **134**, 16413-16423.
- W. Wu, X. Zhang, A. Y. Kornienko, G. A. Kumar, D. Yu, T. J. Emge, R. E. Riman and J. G. Brennan, *Inorg. Chem.*, 2018, **57**, 1912-1918.
- S. Luo, E. Zhang, Y. Su, T. Cheng and C. Shi, *Biomaterials*, 2011, **32**, 7127-7138.
- A. D'Aleo, A. Bourdolle, S. Brustlein, T. Fauquier, A. Grichine, A. Duperray, P. L. Baldeck, C. Andraud, S. Brasselet and O. Maury, *Angew. Chem. Int. Ed.*, 2012, **51**, 6622-6625.
- A. Foucault-Collet, K. A. Gogick, K. A. White, S. Villette, A. Pallier, G. Collet, C. Kieda, T. Li, S. J. Geib, N. L. Rosi and S. Petoud, *Proc. Natl. Acad. Sci. U. S. A.*, 2013, **110**, 17199-17204.
- A. Foucault-Collet, C. M. Shade, I. Nazarenko, S. Petoud and S. V. Eliseeva, *Angew. Chem. Int. Ed.*, 2014, **53**, 2927-2930.
- I. Martinic, S. V. Eliseeva, T. N. Nguyen, V. L. Pecoraro and S. Petoud, *J. Am. Chem. Soc.*, 2017, **139**, 8388-8391.
- M. A. Alcalá, C. M. Shade, H. Uh, S. Y. Kwan, M. Bischof, Z. P. Thompson, K. A. Gogick, A. R. Meier, T. G. Strein, D. L. Bartlett, R. A. Modzelewski, Y. J. Lee, S. Petoud and C. K. Brown, *Biomaterials*, 2011, **32**, 9343-9352.
- Esther M. Surender, S. Comby, B. L. Cavanagh, O. Brennan, T. C. Lee and T. Gunnlaugsson, *Chem*, 2016, **1**, 438-455.
- W. Yang, L. M. Fu, X. Wen, Y. Liu, Y. Tian, Y. C. Liu, R. C. Han, Z. Y. Gao, T. E. Wang, Y. L. Sha, Y. Q. Jiang, Y. Wang and J. P. Zhang, *Biomaterials*, 2016, **100**, 152-161.

ARTICLE

Journal Name

- 32 H. Ma, B. Song, Y. Wang, D. Cong, Y. Jiang and J. Yuan, *Chem. Sci.*, 2017, **8**, 150-159.
- 33 A. T. Frawley, H. V. Linford, M. Starck, R. Pal and D. Parker, *Chem. Sci.*, 2018, **9**, 1042-1049.
- 34 S. Comby and J. C. G. Bünzli, *Lanthanide near-infrared luminescence in molecular probes and devices*, Elsevier, Amsterdam, 2007.
- 35 V. Pansare, S. Hejazi, W. Faenza and R. K. Prud'homme, *Chem. Mater.*, 2012, **24**, 812-827.
- 36 S. J. Bradberry, A. J. Savyasachi, M. Martinez-Calvo and T. Gunnlaugsson, *Coord. Chem. Rev.*, 2014, **273-274**, 226-241.
- 37 J. Y. Hu, Y. Ning, Y. S. Meng, J. Zhang, Z. Y. Wu, S. Gao and J. L. Zhang, *Chem. Sci.*, 2017, **8**, 2702-2709.
- 38 J. Y. Hu, Z. Y. Wu, K. Chai, Z. S. Yang, Y. S. Meng, J. Zhang and J. L. Zhang, *Inorg. Chem. Front.*, 2017, **4**, 1539-1545.
- 39 Y. Ning, J. Tang, Y. W. Liu, J. Jing, Y. Sun and J. L. Zhang, *Chem. Sci.*, 2018, **9**, 3742-3753
- 40 Y. Ning, S. Cheng, J.-X. Wang, Y.-W. Liu, W. Feng, F. Li and J.-L. Zhang, *Chem. Sci.*, 2019, **10**, 4227-4235.
- 41 F. Ding, Y. Zhan, X. Lu and Y. Sun, *Chem. Sci.*, 2018, **9**, 4370-4380.
- 42 Z. M. Tao, G. S. Hong, C. Shinji, C. X. Chen, S. Diao, A. L. Antaris, B. Zhang, Y. P. Zou and H. J. Dai, *Angew. Chem. Int. Ed.*, 2013, **52**, 13002-13006.
- 43 R. Xiong, D. Mara, J. Liu, R. Van Deun and K. E. Borbas, *J. Am. Chem. Soc.*, 2018, **140**, 10975-10979.
- 44 H. J. Yvon, *A Guide to Recording Fluorescence Quantum Yields*, HORIBA Jobin Yvon Inc, Stanmore, Middlesex, UK, 2012.